The Impact of Mixed Negative Bias Temperature Instability and Hot Carrier Stress on Single Oxide Defects

B. Ullmann[*], *M. Jech*[*], *S. Tyaginov*[*] [°], *M. Waltl*[*], *Y. Illarionov*[*] [°], *A. Grill*[*], *K. Puschkarsky*[•], *H. Reisinger*[•], *T. Grasser*[*]

[*]Institute for Microelectronics, TU Wien, Austria [°] Ioffe Physical-Technical Institute, St. Petersburg, Russia
[•] Infineon, Munich, Germany

***Abstract*— Even though transistors are rarely subjected to idealized bias temperature instability or hot carrier stress conditions in circuits, there is only a limited number of studies available on mixed bias temperature instability and hot carrier stress. Here we summarize the results of the first study of mixed negative bias temperature instability and hot carrier stress (drain stress voltage $|V_D^{str}| > 0\,V$ and gate stress voltage $|V_G^{str}| \geq |V_{DD}|$) at the single oxide defect level in nano-scale SiON pMOSFETs. We found that less defects contribute to a threshold voltage shift ΔV_{th} during recovery and thus to the recoverable degradation than would be expected from a simple electrostatic model. Time-dependent defect spectroscopy measurements show that even defects at the source side of the oxide can remain neutral after mixed negative bias temperature instability and hot carrier stress although they are fully charged after homogeneous negative bias temperature instability stress. As a consequence, they do not contribute to a ΔV_{th} drift after mixed negative bias temperature instability and hot carrier stress. We show that this unexpected reduction in the defect's occupancy can be consistently explained by non-equilibrium processes induced by the large drain voltage such as impact ionization.**

I. Introduction

The international technology roadmap for semiconductors (ITRS) lists bias temperature instability (BTI) and hot-carrier degradation (HCD) as most difficult challenges which should be properly understood and modeled [1]. Although extensive experimental and theoretical studies of these phenomena have been performed [2–8] there are still open issues in understanding the nature and behavior of defects contributing to BTI and HCD. Even more dramatic, in circuits transistors are rarely subjected to idealized BTI (gate stress voltage $|V_G^{str}| \gg 0\,V$ and drain stress voltage $V_D^{str} = 0\,V$) or hot carrier (HC) (low $|V_G^{str}|$, $V_D^{str} \geq |V_{DD}|$) conditions. Nevertheless, only a limited number of studies is available on mixed BTI/HC stress [9–12].

For a more realistic life time prediction it is necessary to extend existing models towards mixed NBTI/HC conditions. We focus on the impact of mixed NBTI/HC stress on single oxide defects in order to characterize recoverable device degradation, such as ΔV_{th} drift, in a more general way including $|V_D^{str}| > 0\,V$.

It has been proposed that structural defects in the insulator can capture and emit single charge carriers at certain characteristic times [4]. Charge exchange events of active defects contribute discrete steps of a particular height to the shift of the threshold voltage ΔV_{th} during operation and thus contribute to degradation. The activity of a defect is predetermined by its energy level within the band gap of the insulator. If the level is located in a particular area in the band gap, it can be shifted above the Fermi level by applying a stress gate bias (higher oxide field E_{ox}) and below the Fermi level by applying a recovery gate bias (lower E_{ox}). This area is the active energy region (AER) defined in [4].

Depending on the detailed defect configuration the defect can capture a charge carrier at a capture time τ_c after shifting

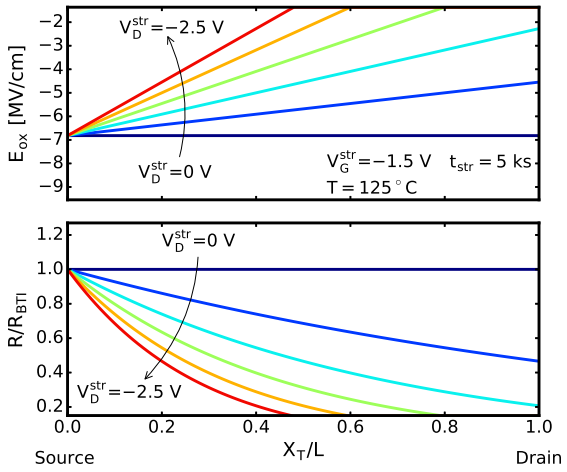

Fig. 1: Simple electrostatic model: Estimation of the ΔV_{th} drift during recovery measurements, here defined as $R = |\Delta V_{th}(t_{rec} = t_{rec}^{min}) - \Delta V_{th}(t_{rec} = t_{rec}^{max})|$, according to [10]. **Top:** E_{ox} decreases linearly from source to drain for $V_D^{str} \leq 0\,V$ but remains unaffected at the source position due to the linear approximation of the channel potential $V_{ch}^{str}(X_T) = V_D^{str} \times X_T/L$. **Bottom:** Relative ΔV_{th} drift R/R_{BTI}. The source side contributes more to the ΔV_{th} drift during recovery measurements than the drain side.

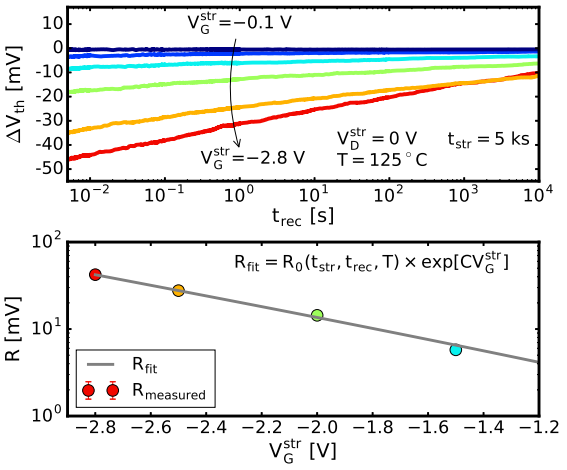

Fig. 2: R after NBTI stress: An electrostatic model according to [10] fits the behavior of R after NBTI stress in large area devices. **Top:** Recorded recovery traces after NBTI stress. **Bottom:** ΔV_{th} drift $R = \Delta V_{th}(t_{rec} = 5\,ms) - \Delta V_{th}(t_{rec} = 10\,ks)$. The model is in agreement with experimental data.

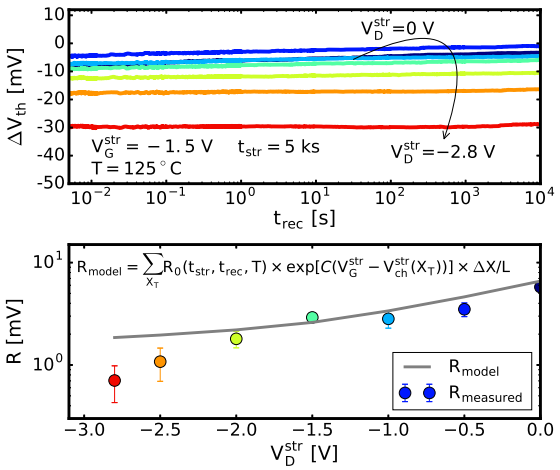

Fig. 3: R after mixed NBTI/HC stress: A discrepancy of R_{measured} compared to R_{model} can be seen in measurements on large area devices. **Top:** Recorded traces after mixed NBTI/HC stress. **Bottom:** ΔV_{th} drift during recovery $R = \Delta V_{\text{th}}(t_{\text{rec}} = 5\,\text{ms}) - \Delta V_{\text{th}}(t_{\text{rec}} = 10\,\text{ks})$. Especially at $V_{\text{D}}^{\text{str}} = -0.5\,\text{V}$ and $V_{\text{D}}^{\text{str}} < -2\,\text{V}$ the measurement points show a lower R than predicted by the simple electrostatic model.

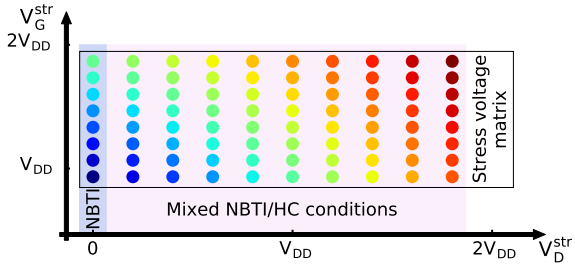

Fig. 4: Stress voltage matrix: TDDS stress and recovery cycles were performed at different stress and recovery conditions at a constant temperature for each device. The stress voltage matrix as a 2-dimensional parameter space with combinations of $V_{\text{D}}^{\text{str}}$ and $V_{\text{G}}^{\text{str}}$ shows the mixed NBTI/HC stress conditions used in this study. The color coding indicates the stress growth and therefore the expected device degradation from "low" (blue) to "high" (red) stress.

its energy level above the Fermi level. Furthermore, it can emit it at an emission time τ_{e} after shifting the energy level below the Fermi level again. Such transitions have been accurately described by non-radiative multiphonon processes [13–15]. In measurements of large area devices the ΔV_{th} step heights cannot be resolved due to the small impact of one charge exchange event between oxide and channel considering the amount of charge carriers in the channel. By contrast, in nano-scale MOSFETs containing a handfull of traps and having a small area such events cause unique measurable ΔV_{th} steps [16, 17]

Using a simple electrostatic model for large area devices the threshold voltage shift with respect to the lateral position has been estimated to be equal to $\Delta V_{\text{th}}(X_T) = V_0(t_{\text{str}}) \times \exp[C(V_{\text{G}}^{\text{str}} - V_{\text{ch}}^{\text{str}}(X_T))]$ [10]. There, $V_{\text{ch}}^{\text{str}}(X_T) = V_{\text{D}}^{\text{str}} \times X_T/L$ is a linear approximation of the channel potential under stress at positions where the condition of inversion is fulfilled. $V_{\text{ch}}(X_T) = (V_{\text{G}}^{\text{str}} - V_{\text{th}}) \times X_T/(L - L_{\text{sat}})$ is the channel potential at the pinch-off point, V_0 is a stress time and temperature dependent constant and C a technology dependent constant. As can be seen in Figure 1 (top), this estimation leads to a lateral position dependent oxide field E_{ox} for $V_{\text{D}}^{\text{str}} < 0\,\text{V}$, which is reduced from source to drain. The result is a deformation of the AER along the channel which means a reduction of the AER from source to drain. With a smaller AER, less defects capture and emit charge carriers and contribute to a ΔV_{th} drift. Figure 1 (bottom) shows this behavior qualitatively. As the most important consequence, the source side is expected to contribute more to the ΔV_{th} drift during recovery measurements than the drain side.

Measurements on large area devices shown in Figures 2 and 3 demonstrate that the estimation of $\Delta V_{\text{th}}(X_T)$ fits and describes the behavior of the ΔV_{th} drift during recovery measurements, here abbreviated R, rather well. Nevertheless, a discrepancy of the measured R compared to the modeled one for $V_{\text{D}}^{\text{str}} \approx -0.5\,\text{V}$ and $V_{\text{D}}^{\text{str}} \leq -2\,\text{V}$ is clearly visible in Figure 3. Measurements in [9] also show that R after mixed NBTI and HC stress can even be negligibly small. This would mean that almost no oxide defects contribute to ΔV_{th}. Since these defects are uniformly distributed all over the device area, such a behavior can not be explained by only an inhomogeneous E_{ox} which would remain nearly unaffected at the source side.

In order to gain insight into the particular capture and emission processes during and after mixed NBTI/HC stress, we characterized τ_{e}, τ_{c}, the occupancy and the step height behavior of single defects in nano-scale MOSFETs for different combinations of stress voltages.

II. Experimental

We use 2.2nm SiON pMOSFETs of a 130nm commercial technology (large area devices: $W = 10\,\mu\text{m}$, $L = 120\,\text{nm}$; nano-scale devices: $W = 160\,\text{nm}$, $L = 120\,\text{nm}$). The MOSFETs are either mounted on ceramic packages or measured directly on-chip. Their temperature is controlled by a computer-controlled furnace or thermo chuck, respectively.

The time dependent defect spectroscopy (TDDS) framework [18] was used to characterize nine single defects in four different nano-scale MOSFETs using stress measure (recovery) sequences at different stress and recovery conditions. The defect characteristics τ_{e}, τ_{c}, the occupancy and the step height were measured. The stress voltage matrix used for the defect capture behavior characterization can be seen schematically in Figure 4.

For each combination of $V_{\text{D}}^{\text{str}}$ and $V_{\text{G}}^{\text{str}}$ as well as $V_{\text{D}}^{\text{rec}}$ and $V_{\text{G}}^{\text{rec}}$ 100 stress measure sequences were performed and the ΔV_{th} drift was measured simultaneously. Figures 5 and 6 show six of 100 recovery traces after four different combinations of $V_{\text{D}}^{\text{str}}$ and $V_{\text{G}}^{\text{str}}$ as representatives of approximately 45000 recorded recovery traces. They contain the typical steps due to charge exchange events between the channel and the oxide caused by single oxide defects. Each defect causes steps with a particular step height at a particular mean value of τ_{e}. By assigning the unique steps to a defect (implied by ellipses in Figures 5 and 6), parameters like τ_{e}, τ_{c} and the occupancy can be extracted as described in [18] and [4].

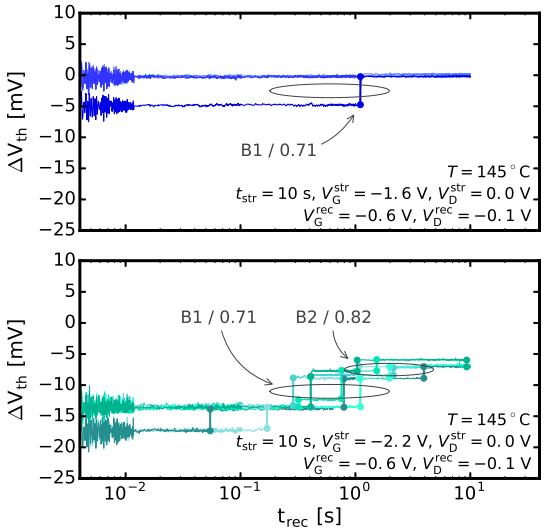

Fig. 5: Recovery traces after NBTI stress measured on device B: Six of 100 recovery traces representatively show the behavior of the unique steps caused by single defects. In this device two defects were fully characterized, B1 and B2. **Top:** B2 does not capture a charge carrier and thus does not emit one during recovery measurements at $V_G^{str} = -1.6\,V$. Only one emission event of B1 can be observed here. **Bottom:** At $V_G^{str} = -2.2\,V$, B1 and B2 capture a charge carrier in 60 % and 50 % of the stress sequences, respectively. This percentage is called occupancy. Emission events of both can be observed in the recovery traces. The percentage of emission events is not scaled linearly since only six of the 100 recorded traces are shown here.

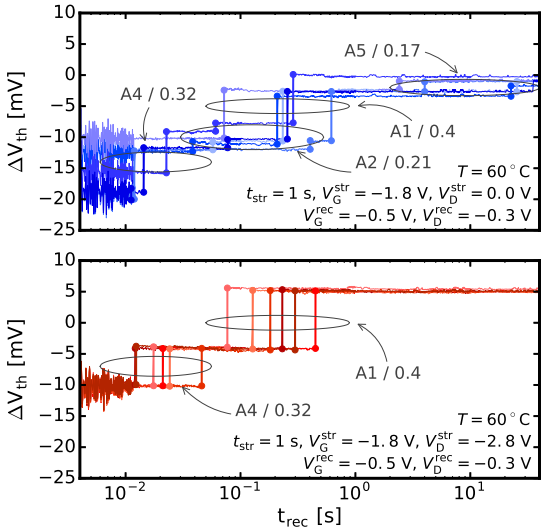

Fig. 6: Recovery traces after mixed NBTI/HC stress measured on device A: Six of 100 recovery traces representatively show the behavior of the unique steps caused by single defects. In this device four defects were fully characterized, A1, A2, A4 and A5. **Top:** At $V_G^{str} = -1.8\,V$ and $V_D^{str} = 0\,V$ all four defects capture a charge carrier during stress and the emission events can be observed in the recovery trace. **Bottom:** At $V_G^{str} = -1.8\,V$ and $V_D^{str} = -2.8\,V$ A2 and A5 cannot be observed in the recovery traces.

III. Results and Discussion

The question to answer was whether the defect properties, especially the capture behavior, correlate with their lateral position in the oxide. In the following, we separate the nine defects into three types: a blue, a green and a magenta group. The reason for this separation is that the defects of each group

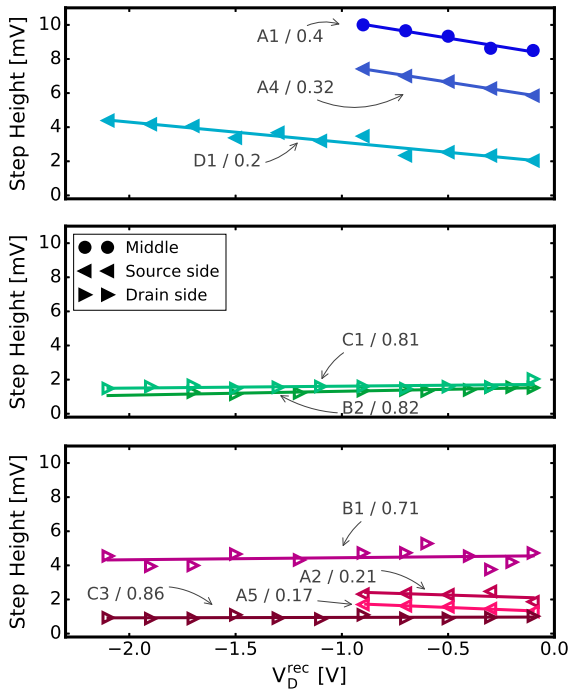

Fig. 7: Extraction of the lateral position: The lateral position X_T/L (0 at source, 1 at drain) was extracted by exploiting the recovery drain bias dependence of the step heights for constant gate recovery voltage V_G^{rec} [19]. The uncertainty of X_T/L is about 20 %. Measurement data and linear fits are labeled with the defect name and the extracted lateral position. The subfigures show the separation of the defects into three types according to their capture behavior during mixed NBTI/HC stress: blue group, green group and magenta group.

have similar capture behaviors during mixed NBTI/HC stress conditions. A more detailed discussion about this follows below.

First, we extracted the relative lateral position X_T/L by exploiting the recovery drain bias dependence of the ΔV_{th} step heights of the defects (see Figure 7). According to simulations considering different random dopant configurations [19], this dependence can be linearly fitted in a simplified way. X_T/L can then be calculated with equation (2) in [19]: $X_T/L = 0.5 - \mathrm{sign}(P_1)\sqrt{2\alpha^2 \log(P_{0max}/P_0)}$. P_0 is the intercept and P_1 is the slope of the linear fit. In our case $P_{0max} = 10\,mV$ because these were the largest step heights observed corresponding to defects in the middle of the channel. α is found to be approximately 0.17 based on the simulations in [19]. The results of the lateral position extraction can be found in Figure 7. Measurement data and linear fits are labeled with the defect name and the extracted relative lateral position X_T/L, e.g., A1 / 0.4. Figure 8 shows the defect distribution in the oxide schematically.

Second, the capture behavior was obtained using the approach described in [18]. In NBTI measurements the defects show a typical capture behavior as can be seen in Figures 5 and 9. By increasing $|V_G^{str}|$ the probability that a defect captures a charge carrier during stress increases. Thus the occupancy grows while τ_c reduces. For example, defect B2 does not capture a charge carrier at $V_G^{str} = -1.6\,V$, and thus no emission event can be seen in the recovery trace in Figure 5 (top). By

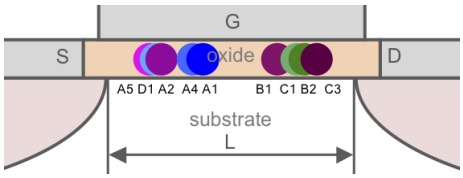

Fig. 8: Lateral defect distribution: Schematic sketch of the positions of the nine characterized defects within the oxide. No clear correlation of the V_D dependence and the location can be observed.

contrast, at $V_G^{str} = -2.2\,V$ B2 captures a charge carrier in 50 % of the stress sequences. This percentage is called occupancy.

In mixed NBTI/HC measurements at a fixed V_G^{str} (around $-2\,V$) and increasing $|V_D^{str}|$ the defects can be separated into three groups according to their occupancy trace in Figure 10. Either the occupancy is constant for the whole V_D^{str} range (defects A1, D1 and A4 – blue group, Figure 10a top) or it decreases for $V_D^{str} < 0\,V$ (C1 and B2 – green group, Figure 10b top) or it shows a local minimum at $V_D^{str} \approx -0.8\,V$, a local maximum at $V_D^{str} \approx -1.5\,V$ and decreases to zero for $V_D^{str} < -1.5\,V$ (C3, B1, A5 and A2 – magenta group, Figure 10c top). The extracted τ_c (Figures 10a, 10b and 10c bottom) with respect to the drain bias shows a slightly increasing trend only for the green group. For the magenta and blue groups τ_c is either constant or decreasing.

The green and blue groups behave as expected. Drain-side defects show a decreasing occupancy and increasing τ_c for mixed NBTI/HC stress. Source-side to mid-channel defects show a constant occupancy over the whole V_D^{str} range. Defects in the magenta group show an unexpected behavior. Quite remarkably, two defects of the magenta group near the source show an occupancy decrease for $V_D^{str} < -2\,V$, A2 and A5. In Figure 6 we compare the recovery traces after NBTI and mixed NBTI/HC stress for all A defects. While the top subfigure shows traces c all four defects, A1, A2, A4 and A5 after NBTI stress, the bottom subfigure shows that A2 and A5 do not emit charge carriers after mixed NBTI/HC stress within the measurement window.

The different behavior of the green and the magenta group can be summarized by mapping the occupancy onto τ_c for a constant V_G^{str} for NBTI stress and for a constant V_D^{str} for mixed NBTI/HC stress (see Figure 11). The traces for increasing $|E_{ox}|$ during NBTI stress and increasing $|V_D^{str}|$ during mixed NBTI/HC stress follow reverse trends for the green group. This means that the occupancy increases and τ_c decreases for increasing $|E_{ox}|$ while the occupancy decreases and τ_c increase for increasing $|V_D^{str}|$. Thus we can conclude that an inhomogeneous E_{ox} affects these defects as discussed in the introduction. By contrast, the magenta group shows a different behavior for increasing $|V_D^{str}|$. For these defects, increasing $|V_D^{str}|$ causes a decrease in both, occupancy and τ_c. This can not be simply explained by the effect of an inhomogeneous E_{ox}.

The considerable reduction in occupancy for the magenta group can be explained by a significant decrease of τ_e with increasing $|V_D^{str}|$. If $\tau_e \ll \tau_c$ at stress conditions, the defect captures a charge carrier but immediately emits it before switching to recovery conditions. Thus the occupancy is reduced and the defect does not contribute to the overall ΔV_{th}.

The result is that, depending on their detailed configuration, defects at all lateral positions can remain neutral after mixed NBTI/HC stress. To explain such a complex behavior, additionally to an inhomogeneous E_{ox} also non-equilibrium processes induced by the high $|V_D^{str}|$ have to be taken into account.

IV. Capture and Emission Times under Mixed NBTI/HC Conditions

Under BTI conditions ($|V_G^{str}| \gg 0\,V$ and $V_D^{str} = 0\,V$) the carriers in the channel are in equilibrium and thus properly described by a Boltzmann distribution. As soon as a drain bias is applied this approximation is no longer valid. Carriers can gain energy due to various mechanisms and can be severely out of equilibrium. Thus a thorough carrier transport treatment by means of an exact solution of the Boltzmann transport equation is needed for such situations. Furthermore, if the device is operated near or beyond pinch-off conditions (high V_D^{str}) carriers with sufficient kinetic energy can trigger impact ionization (II). It has been recently shown that the majority carriers can significantly change the degradation characteristics [20, 21].

The impact of II on τ_c and τ_e depends strongly on the particular configuration and on the lateral position of the defect. Figure 12 shows a comparison of the characteristic capture and emission times during NBTI and mixed NBTI/HC stress for $V_G^{str} = -1.5\,V$ for defect B1. Here τ_c and τ_e are first modeled using the non-radiative multiphonon model [4] assuming equilibrium carriers in the channel and show an increasing trend simply due to the change of E_{ox} at this lateral position (dashed lines). This does not correspond to the measurement data of B1. Figure 10c shows that the occupancy of B1 decreases for $V_D^{str} \leq -1.5\,V$ while τ_c shows a slightly decreasing trend. Furthermore, the experimental data for the drain voltage dependence of τ_e in Figure 12 clearly exposes a decreasing behavior with $V_D^{str} < 0\,V$. Only if the non-equilibrium conditions are correctly considered by taking into account II via a solution of the Boltzmann transport equation we obtain agreement with experimental data (solid lines).

As a result, τ_c and τ_e modeled with respect to a full non-equilibrium model show a good agreement with the measured τ_e of B1. At the same time the reduction in occupancy due to $\tau_e \ll \tau_c$ for $V_D^{str} \leq -1.5\,V$ is described properly. Under these conditions, the defect captures a charge carrier during stress but emits it immediately and therefore remains neutral after stress. This approach fully explains the experimental observations.

V. Conclusions

We have characterized nine single oxide defects in nano-scale MOSFETs in order to observe their behavior during mixed NBTI/HC. Some defects have shown the expected behavior as a consequence of an inhomogeneous electric field in the oxide: drain-side defects have remained neutral and

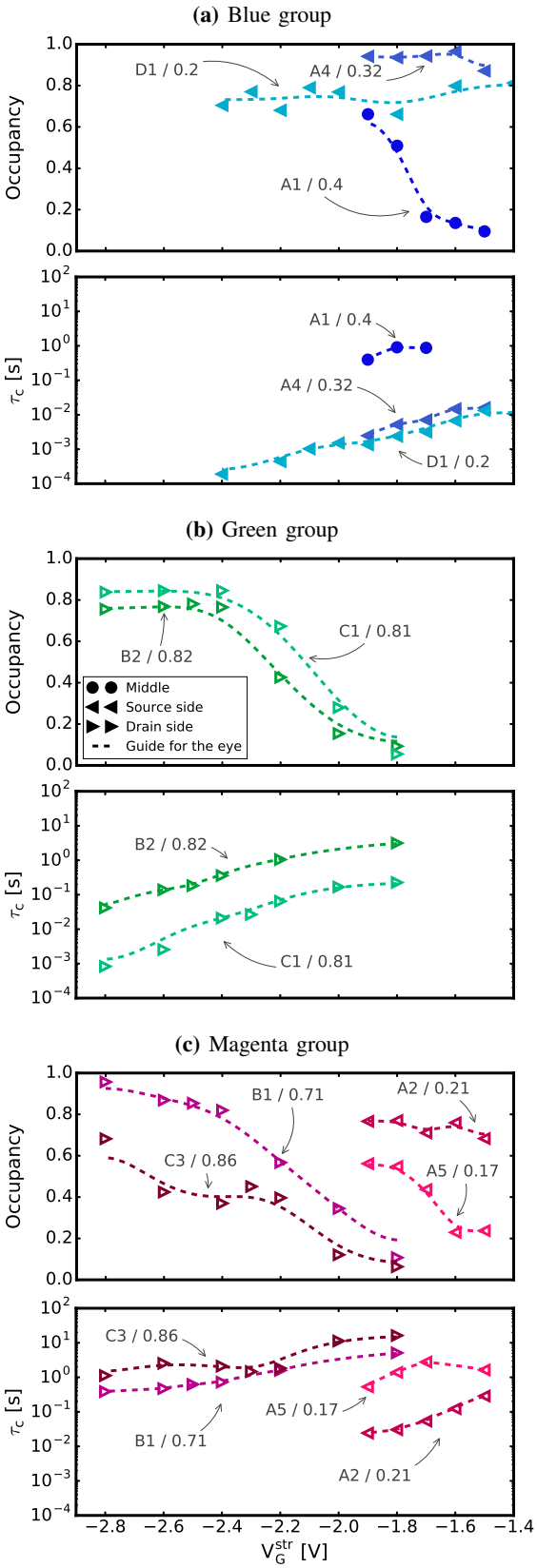

Fig. 9: Capture characteristics at NBTI stress ($V_D^{str} = 0\,V$): The defects show a typical behavior. By increasing $|V_G^{str}|$ the probability that a defect captures a charge carrier during stress increases. The occupancy of the defects increases for increasing $|V_G^{str}|$. τ_c extracted according to [18] decrease for increasing $|V_G^{str}|$.

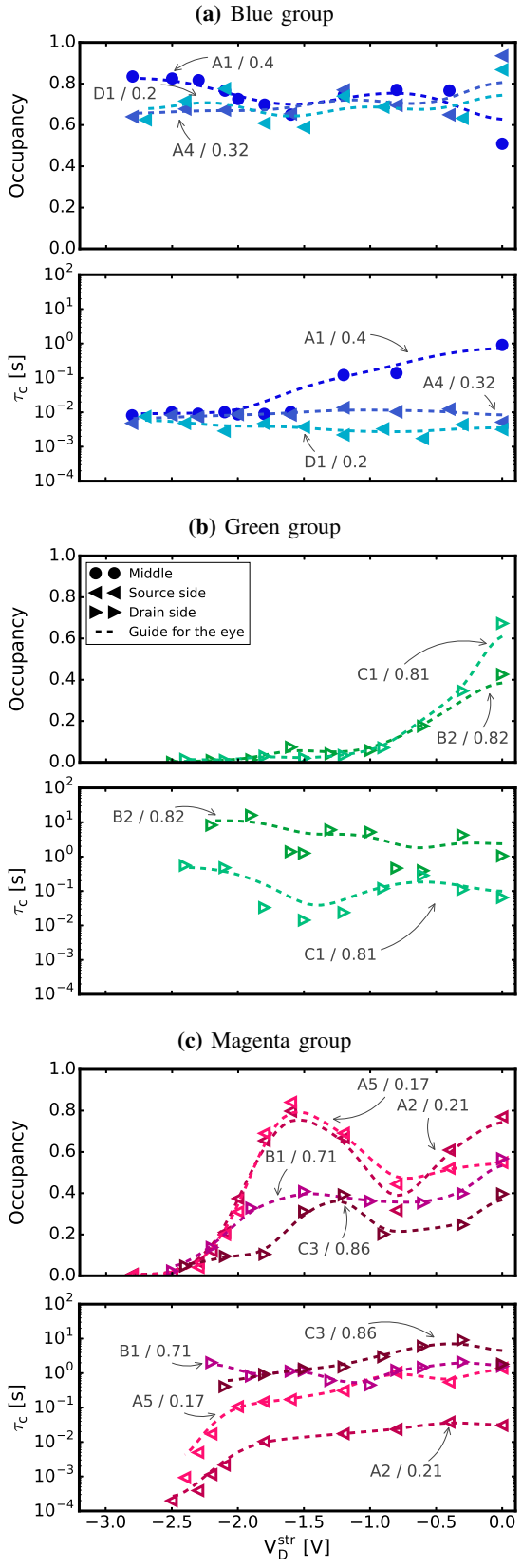

Fig. 10: Capture characteristics at mixed NBTI/HC stress: Occupancy of the defects, characterized for different V_D^{str} at constant $V_G^{str} \approx -2\,V$ (device dependent), exposes three defect types: (a) the blue group (occupancy nearly constant for whole V_D^{str} range), (b) the green group (decreasing occupancy for $V_D^{str} < 0\,V$) and (c) the magenta group (occupancy shows local minimum at $V_D^{str} \approx -0.8\,V$, a local maximum at $V_D^{str} \approx -1.5\,V$ and decreases to zero for $V_D^{str} < -1.5\,V$). In (b) τ_c increases slightly, in (a) and (c) τ_c is either constant or decreases.

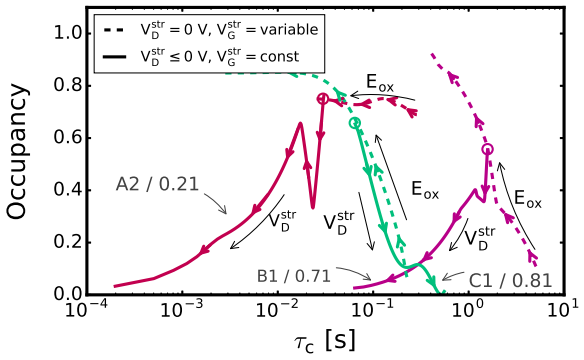

Fig. 11: Occupancy versus capture time: traces for three defects, one of the green group and two of the magenta group. **Dashed lines:** For NBTI stress the ocupancy increases and τ_c decreases for increasing E_{ox}. **Solid lines:** As soon as V_G^{str} and thus E_{ox} is held at a constant value and $V_D^{str} < 0$ V, the occupancy of the green defects shows a reverse trend compared to NBTI - the occupancy decreases and τ_c increases. By contrast, the occupancy of the magenta defects follows a trace towards decreasing τ_c for a decreasing occupancy.

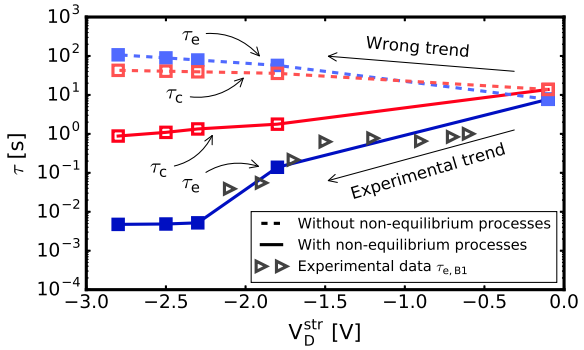

Fig. 12: Comparison of τ_c and τ_e: Dashed lines: τ_c and τ_e modeled using the non-radiative multiphonon model [4] assuming equilibrium carriers in the channel which show an increasing trend simply due to the change of E_{ox}. **Solid lines:** τ_c and τ_e modeled considering non-equilibrium conditions by taking into account impact ionization during the solution of Boltzmann's transport equation which results in agreement with the experimental data. As soon as $\tau_e \ll \tau_c$, the defect captures a charge carrier during stress but emits it immediately. Thus such defects do not contribute to the overall ΔV_{th}.

source-side and middle defects have remained unaffected. Surprisingly, other defects have shown an unexpected behavior. Two source-side defects have remained neutral at high $|V_D^{str}|$ and did not contribute to ΔV_{th}, which cannot be explained by the inhomogeneous electric field alone.

The explanation for this is a significant decrease of τ_e compared to τ_c at increasing $|V_D^{str}|$ due to non-equilibrium processes triggered by hot carriers with sufficient energies: the defect captures a charge carrier during stress conditions but emits it immediately and remains neutral after stress. Thus, depending on their detailed configuration, defects at all lateral positions can remain neutral after mixed NBTI/HC stress and thus not contribute to ΔV_{th}.

Acknowledgments

The research leading to these results has received funding from the Austrian Science Fund (FWF) projects n° P 26382-N30, P 23958-N24 and I2606-N30 and from the European Union FP7 project ATHENIS 3D (Grant n° 619246).

References

[1] "More Moore," in *International Technology Roadmap for Semiconductors*. Semiconductor Industry Association, 2015, ch. 5.

[2] V. Huard, M. Denais, F. Perrier, N. Revil, C. Parthasarathy, A. Bravaix, and E. Vincent, "A Thorough Investigation of MOSFETs NBTI Degradation," *Microelectronics Reliability*, vol. 45, pp. 83–98, 2005.

[3] D. Schroder, "Negative Bias Temperature Instability: What Do We Understand?" *Microelectronics Reliability*, vol. 47, no. 6, pp. 841–852, 2007.

[4] T. Grasser, "Stochastic Charge Trapping in Oxides: From Random Telegraph Noise to Bias Temperature Instabilities," *Microelectronics Reliability*, vol. 52, pp. 39–70, 2012.

[5] A. Bravaix and V. Huard, "Hot-Carrier Degradation Issues in Advanced CMOS Nodes," in *Proc. European Symposium on Reliability of Electron Devices (ESREF)*, 2010, pp. 1267–1272.

[6] S. Tyaginov and T. Grasser, "Modeling of Hot-Carrier Degradation: Physics and Controversial Issues," in *Proc. International Integrated Reliability Workshop (IIRW)*, 2012, pp. 206–215.

[7] S. Tyaginov, I. Starkov, H. Enichlmair, J. Park, C. Jungemann, and T. Grasser, "Physics-Based Hot-Carrier Degradation Models," *ECS Transactions*, vol. 35, no. 4, pp. 321–352, 2011.

[8] S. Rauch and G. L. Rosa, "CMOS Hot Carrier: From Physics to End of Life Projections, and Qualification," in *Proc. International Reliability Physics Symposium (IRPS), tutorial*, 2010.

[9] G. Rott, K. Rott, H. Reisinger, W. Gustin, and T. Grasser, "Mixture of Negative Bias Temperature Instability and Hot-Carrier Driven Threshold Voltage Degradation of 130 nm Technology p-Channel Transistors," *Microelectronics Reliability*, vol. 54, no. 9-10, pp. 2310–2314, 2014.

[10] C. Schlünder, R. Brederlow, B. Ankele, W. Gustin, K. Goser, and R. Thewes, "Effects of Inhomogeneous Negative Bias Temperature Stress on p-Channel MOSFETs of Analog and RF Circuits," *Microelectronics Reliability*, vol. 45, no. 1, pp. 39 – 46, 2005.

[11] J. Franco and B. Kaczer, "Channel Hot Carriers in SiGe and Ge pMOSFETs," in *Hot Carrier Degradation in Semiconductor Devices*, T. Grasser, Ed. Springer-Verlag, 2015, ch. 9, pp. 259–285.

[12] F. Cacho, P. Mora, W. Arfaoui, X. Federspiel, and V. Huard, "HCI/BTI Coupled Model: The Path for Accurate and Predictive Reliability Simulations," in *Proc. International Reliability Physics Symposium (IRPS)*, 2014, pp. 5D.4.1–5D.4.5.

[13] M. Kirton and M. Uren, "Noise in Solid-State Microstructures: A New Perspective on Individual Defects, Interface States, and Low-Frequency (1/f) Noise," *Advances in Physics*, vol. 38, no. 4, pp. 367 – 486, 1989.

[14] K. Huang and A. Rhys, "Theory of Light Absorption and Non-Radiative Transitions in F-Centres," *Proc. Royal Society A*, vol. 204, pp. 406–423, 1950.

[15] C. Henry and D. Lang, "Nonradiative Capture and Recombination by Multiphonon Emission in GaAs and GaP," *Physical Review B*, vol. 15, no. 2, pp. 989–1016, 1977.

[16] A. Ghetti, C. M. Compagnoni, A. S. Spinelli, and A. Visconti, "Comprehensive Analysis of Random Telegraph Noise Instability and Its Scaling in Deca-Nanometer Flash Memories," *IEEE Transactions on Electron Devices*, vol. 56, no. 8, pp. 1746–1752, 2009.

[17] J. Franco, B. Kaczer, M. Toledano-Luque, P. J. Roussel, L. A. R. J. Mitard, L. Witters, T. Chiarella, M. Togo, N. Horiguchi, and G. Groeseneken, "Impact of Single Charged Gate Oxide Defects on the Performance and Scaling of Nanoscaled FETs," in *Proc. International Reliability Physics Symposium (IRPS)*, 2012, pp. 1 – 6.

[18] T. Grasser, H. Reisinger, P.-J. Wagner, F. Schanovsky, W. Goes, and B. Kaczer, "The Time Dependent Defect Spectroscopy (TDDS) for the Characterization of the Bias Temperature Instability," in *Proc. International Reliability Physics Symposium (IRPS)*, 2010, pp. 16 – 25.

[19] Y. Illarionov, M. Bina, S. Tyaginov, K. Rott, B. Kaczer, H. Reisinger, and T. Grasser, "Extraction of the Lateral Position of Border Traps in Nanoscale MOSFETs," *IEEE Transactions on Electron Devices*, vol. 62, no. 9, pp. 2730–2737, 2015.

[20] M. Bina, K. Rupp, S. Tyaginov, O. Triebl, and T. Grasser, "Modeling of Hot Carrier Degradation Using a Spherical Harmonics Expansion of the Bipolar Boltzmann Transport Equation," in *Proc. International Electron Devices Meeting (IEDM)*, 2012, pp. 713 – 716.

[21] S. Tyaginov, I. Starkov, O. Triebl, H. Enichlmair, C. Jungemann, J. Park, H. Ceric, and T. Grasser, "Secondary Generated Holes as a Crucial Component for Modeling of HC Degradation in High-Voltage n-MOSFET," in *Proc. International Conference on Simulation of Semiconductor Processes and Devices (SISPAD)*, 2011, pp. 123 – 126.